JOURNAL OF PROPULSION AND POWER
Vol. 26, No. 4, July–August 2010

Determining Vacuum-Arc Thruster Performance Using a Cathode-Spot Model

J. Lun,* R. T. Dobson,† and W. H. Steyn‡
University of Stellenbosch, Stellenbosch 7602, South Africa

DOI: 10.2514/1.41625

A simple model of the vacuum-arc cathode-spot and plasma region was developed to predict the performance of vacuum-arc thrusters operating roughly in the arc current range 80–300 A with thrust pulses ≥ 250 μs. The conventional-based cathode-spot model predicts ion current, average ion velocity, and erosion rate to establish thruster performance. Vacuum-arc properties for a range of materials (Al, Ti, Cr, Fe, Ni, Cu, Ag, Pb, Bi) were determined as well as maximum arc spot currents for Ti, Cr, Fe, Ni, and Bi. Model results generally show good agreement with published data and predicted thruster performance is comparable to literature. Most values of ion-to-arc current ratio were within 10% of published experimental data, ion velocities within about 30%, and erosion rates were within roughly 50%, provided macroparticle ejection was low. The crucial role of the ion-to-arc current ratio on thruster performance is assessed.

Nomenclature

A_s	=	cathode-spot area, m^2
A_1, A_2, A_3	=	effective work function constants
B	=	spin number
C_T	=	thrust correction factor
E	=	electric field, V/m
E_r	=	erosion rate, μg/C
e	=	electron charge, C
F	=	thrust, N
f	=	fractional ion charge state
G	=	degeneracy
g	=	gravitational acceleration, ms^{-2}
H	=	thrust-to-power ratio, N/W
h	=	Planck's constant, Js
I	=	current, A
I^*	=	maximum spot current, A
I_{sp}	=	specific impulse, s
J	=	current density, Am^{-2}
K_b	=	Boltzmann constant, J/K
K_1, K_2	=	material-dependent pressure constants
k	=	integer
L	=	Lorentz number, $W\Omega K^{-2}$
m	=	mass, kg
N	=	cathode-spot number
n	=	particle density, m^{-3}
P	=	power, W
p	=	pressure, Pa
q	=	energy flux, Wm^{-2}
r_s	=	cathode-spot radius, m
T	=	temperature, K or eV
V_a	=	anode potential drop, V
V_{cs}	=	cathode potential drop, V
V_d	=	arc voltage, V
v	=	velocity, m/s
W	=	energy potential level, eV
Z	=	ion charge state
α	=	backflow coefficient
Γ	=	atom flux density, $m^{-2}\ s^{-1}$
γ	=	degree of ionization
ϵ_o	=	permittivity of free space, $C^2\ N^{-1}\ m^{-2}$
ζ	=	ion-to-arc current ratio
η	=	efficiency
Λ	=	partition function
λ	=	thermal conductivity, $W\ m^{-1}\ K^{-1}$
σ	=	electric conductivity, S/m
ϕ	=	work function, eV
ϕ_{eff}	=	effective field-enhanced work function, eV

Subscripts

b	=	boiling
con	=	conduction
cool	=	cooling the cathode
d	=	discharge
e	=	electron
em	=	emitted electrons
er	=	returning electrons
i	=	ion
J	=	Joule heating
k	=	ion species
n	=	atom, neutral
p	=	plasma
s	=	cathode-spot surface
sh	=	sheath edge
t	=	total
vap	=	vapor, vaporization
Y	=	energy level

Received 21 October 2008; revision received 17 January 2010; accepted for publication 28 February 2010.

*M.Sc. Graduate, Department of Mechanical and Mechatronic Engineering, Western Cape, Private Bag X1, Matieland.

†Senior Lecturer, Department of Mechanical and Mechatronic Engineering, Western Cape, Private Bag X1, Matieland.

‡Professor, Department of Electrical and Electronic Engineering, Western Cape, Private Bag X1, Matieland.

Introduction

THE vacuum-arc thruster (VAT) has been shown to be a potential micropropulsion technology in recent years [1,2]. The novelty of the thruster is its use of any solid conducting propellant (usually metal), low average power (1–100 W), low arc voltage (∼20 V), low system mass (less than 500 g), variable-thrust capability, and high specific impulse (∼500–1000 s). The vacuum-arc thruster consists of anode and cathode electrodes separated by a thin layer of insulation. An arc current is generated between the two electrodes in a gap at the thruster's end, producing plasma from the vaporized cathode metal that accelerates outward as thrust. The arc originates from small localized spots formed on the cathode surface known as

cathode spots. Each spot is able to transport up to a certain amount of arc current (e.g., 75–100 A for copper [3]). For larger arc currents, additional spots are formed on the surface such that the number of spots is proportional to the arc current being delivered. The most typical arc currents and arc pulse lengths of a VAT may range between 50–300 A and 50–500 μs. Usually, an inductive driver or pulse forming network is used to power the thruster [1,2].

There are a number of recent studies devoted to describing VAT performance and behavior. Polk et al. [4] developed a semi-empirical VAT model for a wide range of cathode materials. Their work considered the effect of the ion density distribution and thruster geometry on thrust and relied on an assumed ion-to-arc current ratio and experimentally measured values of ion velocity, average ion charge state, and erosion rate. Statom [5] also developed a model dependent on empirical values and predicted ion velocity with an energy balance, but assumed no ion distribution. Keidar et al. [6] developed a theoretical model of the VAT plasma jet and studied the effect of an external magnetic field on the jet. Rysanek and Burton [7] studied the characteristics of macroparticles emitted from the VAT. Recently, Beilis [8] developed a theoretical model of a short-pulsed VAT. This paper builds upon Polk et al.'s [4] work by presenting a simplified VAT cathode-spot model that predicts the ion current (presented in the form of an ion-to-arc current ratio), ion velocity, and erosion rate to establish thruster performance.

Description of the Vacuum-Arc Cathode-Spot Region

Vacuum arc phenomena are highly complex and despite over a century of study, has yet to be completely described. Early conventional models of vacuum arcs assumed highly simplified arc behavior, such as steady-state processes and circular stationary cathode spots. However, cathode spots are dynamic, open, and fractal systems [9], whose properties fluctuate rapidly to maintain arc conditions, and whose behavior appears to resemble that of complex violent explosions. Therefore, much effort has been done over the last few decades to develop transient, nonstationary vacuum-arc models. However, the complexity of such a task means that a complete theory of vacuum arcs still remains elusive and its aspects highly debated even today [10].

According to the conventional model, the cathode-spot region can generally be separated into four zones: the cathode-spot surface, a positive sheath region, a presheath/ionization zone, and a plasma jet region (Fig. 1). Each zone is characterized by specific energy processes or interactions/general behavior of atoms (a), ions (i), and electrons (e). Joule heating and ion bombardment form high temperature cathode spots at surface microprotrusions, ejecting cathode atoms. Tiny craters are thus formed by the loss of cathode material ($\sim$10–100 μg/C). Over the lifetime of the vacuum-arc cathode spot, growth of these craters decreases Joule heating, and the temperature drops below the point of sustaining vapor and electron emission and the arc site extinguishes. A new site at a nearby microprotrusion is initiated by the molten flow of the previous site.

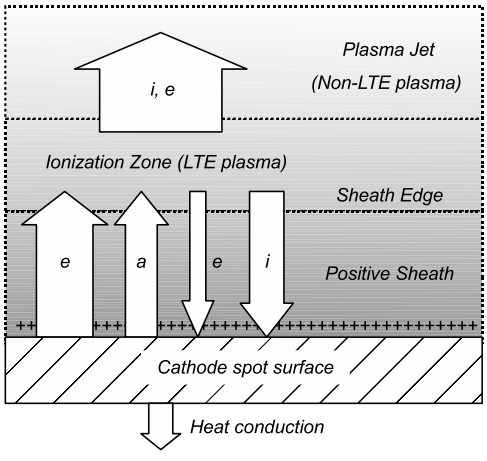

Fig. 1 Illustration of the vacuum-arc cathode-spot region.

During the vacuum arc, a large electric field ($\sim 10^9$ V/m) exists between the electrodes, causing electron field emission at the cathode. In addition, the high temperature of the cathode surface causes electron thermionic emission. The combined effect, known as thermofield (T-F) emission, is necessary for the arc to exist [11]. A cathode potential drop also exists within the cathode-spot region. The large electron flow has enough kinetic energy to ionize nearly all the metal atoms in the ionization zone. The newly created ions have been shown to be multiply charged depending on the arc discharge time [12]. A significant portion of the generated ions accelerate outward together with the electrons as a quasi-neutral plasma jet, producing thrust. Three main ion-accelerating mechanisms have been identified [13,14]: a high-pressure gradient produced from the plasma cloud in front of the cathode, electrostatic attraction of the ions to a negative potential hump formed in front of the cathode spot, and electron–ion friction (electrons imparting momentum to ions by collision). Some of the remaining ions formed are also attracted back to the cathode surface, producing a sheath of positive ions over the cathode surface, which also attracts returning electrons. The flow of returning ions produces a large electric field across the sheath and when they bombard the surface, cause cathode heating. Liquid metal droplets or macroparticles are also ejected from the cathode spot, but travel much slower ($\sim 10^2$ m/s) than the ejected ions ($\sim 10^4$ m/s) [15]. Typical ion current densities and heat fluxes are on the order of 10^{10-12} A/m^2 and 10^{9-13} W/m^2, respectively [4]. Typical plasma densities are on the order of 10^{24-26} m^{-3} and the escaping ion current is about 7–10% of the arc current [4].

Development of the Simplified VAT Model

The model in this work is based on conventional vacuum-arc models, which are limited to: 1) one-dimensionality in the region just above the cathode surface; 2) steady-state processes; and 3) nonrefractory metals, e.g., aluminum, copper. An energy flux balance at the cathode surface is used to find the cathode-spot surface temperature and size, both of which govern much of the processes within the arc [16,17]. The model is applied to single cathode-spot operation, which can then be extended to multispot vacuum-arc operation. The model presented here is currently limited to vacuum arcs roughly occurring in the arc current range $I_d = 80$–300 A and pulse lengths ≥ 250 μs, which are the general limits of the published experimental data that were used as model inputs. However, further experimental results may reveal a wider range of applicability.

Inputs to the model are the cathode material's atomic and thermophysical properties, measured values of maximum spot arc current [3] and measured values of ion charge state distribution (CSD) [18] for arc pulses of 100 A and 250 μs. Anders [19] applied this CSD information to the Saha equation to analytically estimate an electron temperature at which the plasma transitions from LTE to non-LTE conditions during its outward expansion. This is possible because the CSD freezes at this transition point and thus can provide information to the outside world about conditions within the cathode-spot region. Thus, by extension, we also use this electron temperature calculated by Anders [19] as a model input.

Assumptions

In addition, the following assumptions and simplifications are used [11,20]:

1) Arc processes in the cathode region occur along a one-dimensional line normal to the cathode surface plane; i.e., particles only travel to and from the cathode surface.

2) There are steady-state arc processes (startup and shutdown transient nature of the arc are ignored).

3) There are singular, stationary, circular, independent cathode spots on a large, cold cathode body surface (substructures within the spot are ignored).

4) There is a sufficiently smooth, clean cathode surface (the height of surface microprotrusions is much less than the sheath thickness such that the surface appears relatively uniform to the plasma).

5) There is uniform cathode-spot temperature distribution.

6) Energy flux processes are confined by the cathode-spot boundary, i.e., they do not act outside the spot.

7) There is a collisionless, uniformly thick sheath region.

8) There are Maxwellian distributions of ions and electrons.

9) Current flow away from the cathode is defined as positive.

10) The effects of macroparticle/liquid droplet ejection on vacuum-arc processes are ignored.

11) Electron, ion temperatures, and ion charge state distribution are assumed constant in the ionization zone.

12) The plasma in the ionization zone is quasi-neutral and in local thermal equilibrium (LTE).

13) The plasma in the plasma jet region is mainly accelerated by the gasdynamic accelerating mechanism.

14) There is negligible external or internal magnetic field influence on the plasma.

15) Complex feedback effects such as the effect of the plasma on cathode surface properties or on itself are ignored.

Arc Voltage

Applying the cohesive energy rule [21], the arc voltage can be approximated by

$$V_d \approx 14.3 + 1.69 W_{\mathrm{CE}} \tag{1}$$

where W_{CE} is the cohesive energy of the cathode material. Since the cathode potential drop makes up the largest portion of V_d, we assume it to be

$$V_{\mathrm{cs}} \approx V_d - V_a \tag{2}$$

where the anode potential drop is $\sim$1 V.

Atomic Vaporization

The equilibrium vapor pressure is the pressure of the gas atoms at the cathode surface temperature such that the rate of atom condensation and vaporization are equal. The vapor pressure is approximated as [22]

$$\log(p_{\mathrm{vap}}) = K_1 - \frac{K_2}{T_s} \tag{3}$$

where K_1 and K_2 are material constants, T_s is the cathode-spot surface temperature and p_{vap} is in units of torr. The evaporating atom flux density is determined by the Hertz–Knudsen formula as [16,20,23]

$$\Gamma_{\mathrm{vap}} = \frac{p_{\mathrm{vap}}}{4}\left(\frac{m_n K_b T_s}{3}\right)^{-1/2} \tag{4}$$

where m_n is the atom mass and K_b is the Boltzmann constant.

Ion Charge State Distribution

Measurement of ion charge states reveal that they are often multiply charged [13]. The ion CSD is generally independent of arc current [12] and assumed uniform within the jet [4]. The number of ion species created by the arc is found to be material-dependent. For example, aluminum contains a maximum ion species charge of 3^+ ($k = 3$): that is, ionized by the loss of three electrons from the atom's outer orbital cloud. The mean ion charge of the plasma is thus

$$\bar{Z} = \sum_k f_k Z_k \tag{5}$$

where f_k is the fractional portion of ion species k and Z_k is the ion charge state of species k (e.g., $Z_1 = 1$, $Z_2 = 2$, etc.).

Ion Bombardment

Ions formed above the cathode-spot flow back to the cathode surface and bombard it, causing a significant portion of the heat generated there as shown in Fig. 1. The current density of the returning ions is determined by [11]

$$J_i = \sum_k J_{i,k} = \sum_k \alpha \gamma f_k Z_k e \Gamma_{\mathrm{vap}} \tag{6}$$

where γ is the first degree of ionization (discussed later), e is the electron charge and backflow coefficient α is defined as the ratio of ion flow back to the cathode versus ions produced. As a rough approximation, equal portions of produced ions are assumed to travel toward as well as away from the cathode, i.e., $\alpha \approx 0.5$ [11,12].

The ion velocity at the sheath edge is determined by application of the Bohm sheath criterion, which states that the ions must have a minimum velocity toward the cathode to maintain a stable sheath zone. The Bohm criterion is commonly used as a boundary condition between the sheath and ionization zone [16,20,24–26],

$$v_{i,\mathrm{sh}} = \left[\frac{K_b(T_i + T_e)}{m_i}\right]^{1/2} \tag{7}$$

and the ion density at the sheath is

$$n_{i,\mathrm{sh}} = \frac{J_i}{e v_{i,\mathrm{sh}}} \tag{8}$$

where m_i is the ion mass, and T_i and T_e are the ion and electron temperatures at the sheath edge, respectively. Following the approach of Messaad et al. [16], $T_i \approx T_s$.

Electric Field

The electric field may be described by a simplified form of the Mackeown equation [16,23,25,27]:

$$E = \left(\frac{8\bar{Z} m_i J_i^2 V_{\mathrm{cs}}}{e\epsilon_o^2}\right)^{1/4} \tag{9}$$

where ϵ_o is the permittivity of free space. The electric field reduces the cathode material work function ϕ, resulting in an effective field-enhanced work function, otherwise known as the Schottky effect [3,16,20]. An empirical approximation is used within the realm of T-F emission [12]

$$\phi_{\mathrm{eff}} \approx \frac{\phi T_s^2(1 + 2K_b T_s/\phi)(\phi^{3/2} + A_1 E) - A_2 E^2 \phi^{1/2}}{T_s^2(\phi^{3/2} + A_1 E) + A_3 E \phi} \tag{10}$$

where constants $A_1 = 10^{-10}$, $A_2 = 0.85 \times 10^{-12}$ and $A_3 = 0.85 \times 10^{-2}$ are used.

Emitted Electrons

A simplified estimate of Murphy and Good's [28] thermofield electron emission equation is used [12]. However, this equation is only valid for the approximated ranges of $E = 2.5$–7.5×10^9 V/m and $T_s = 2500$–7500 K,

$$J_{\mathrm{em}} \approx (A_T T_s^2 + A_F E^x) \exp\left[-\left(\frac{T_s^2}{B_T} + \frac{E^2}{B_F}\right)^{-1/2}\right] \tag{11}$$

where the constants A_T, A_F, B_T, B_F, and x are a function of ϕ. The emitted electron density at the sheath edge is [20,24]

$$n_{\mathrm{em,sh}} = \frac{J_{\mathrm{em}}}{e}\left(\frac{m_e}{2}\right)^{1/2}(2K_b T_s + eV_{\mathrm{cs}})^{-1/2} \tag{12}$$

where m_e is the electron mass.

Returning Electrons

From the quasi-neutral plasma assumption, the total electron density at the sheath edge is

$$n_{e,\mathrm{sh}} = \bar{Z} n_{i,\mathrm{sh}} \tag{13}$$

The back-diffused/returning electron density is found by a density balance at the sheath edge

$$n_{\mathrm{er,sh}} = n_{e,\mathrm{sh}} - n_{\mathrm{em,sh}} \tag{14}$$

Consequently, the current density of the returning electrons may be described by [24,26,27]

$$J_{\mathrm{er}} = \frac{1}{4} e n_{\mathrm{er,sh}} \left(\frac{8K_b T_e}{\pi m_e}\right)^{1/2} \exp\left(-\frac{eV_{\mathrm{cs}}}{K_b T_e}\right) \tag{15}$$

Arc Current

Consolidating the calculated current densities into a current density balance at the sheath edge gives the total current density for the cathode spot:

$$J_t = J_{\mathrm{em}} - (-J_i) - J_{\mathrm{er}} = J_{\mathrm{em}} + J_i - J_{\mathrm{er}} \tag{16}$$

The arc current for a cathode spot is thus

$$I_t = J_t A_s = J_t(\pi r_s^2) \tag{17}$$

where the cathode-spot area A_s is approximated as a circle of radius r_s. Also defined is an *effective* cathode-spot number as

$$N = \begin{cases} I_d/I^* & (I_t = I^*) \\ 1 & (I_t < I^*) \end{cases} \tag{18}$$

where I_d is the total arc current and I^* is the maximum amount of arc current that a single spot can contain. Arc currents greater than I^* will force additional spots to form on the cathode surface.

Ionization Zone

The plasma electron and ion densities are approximated by means of the *zero-order model* [12,26], which assumes LTE and quasi-neutral plasma. Hence, the electron, ion, and plasma densities, respectively, are

$$n_{e,p} \approx n_{e,\mathrm{sh}} \exp(\tfrac{1}{2}) \tag{19}$$

$$\bar{Z} n_{i,p} = n_{e,p} \tag{20}$$

$$n_p = n_{e,p} + n_{i,p} \tag{21}$$

For simplicity, an ideal gas is assumed to be ionized into singly ionized atom species to produce LTE plasma. Based on the discussions of Pfender [29] and Cambel [30] and the approach of a number of authors [20,24,25], $T_p \approx T_e$. This is valid because the electron temperature ($\sim$20, 000 K) is typically much higher than the ion temperature ($\sim$4000 K). Therefore, T_p will be much closer in value to T_e than T_i. Because of the quasi-neutral plasma assumption, the degree of ionization may be estimated as

$$\gamma = \frac{n_{e,p}}{n_p} = \frac{n_{i,p}}{n_p} \tag{22}$$

The degree of ionization for a *singly* ionized species may be found by applying the Saha equation (only valid for LTE plasma) [30]

$$\frac{\gamma^2}{1-\gamma^2} = \left(\frac{2\pi m_e}{h^2}\right)^{3/2} \frac{(K_b T_p)^{5/2}}{p_p} \frac{2\Lambda_1}{\Lambda_0} \exp\left(\frac{-eW_{i,1}}{K_b T_p}\right) \tag{23}$$

where h is the Planck constant, $W_{i,1}$ is the first ionization energy, the plasma pressure is described using the ideal-gas equation as [30]

$$p_p = n_p K_b T_p \tag{24}$$

and the partition functions of the atom ($Y = 0$) and ion ($Y = 1$) particles are [30]

$$\Lambda_0 = G_0 \tag{25}$$

$$\Lambda_1 = G_0 + G_1 \exp\left(\frac{-eW_{i,1}}{K_b T_p}\right) \tag{26}$$

where the degeneracy may be found from $G_Y = 2B_Y + 1$, where B_Y is the spin number of the atom ($Y = 0$) or ion ($Y = 1$), respectively.

Plasma Jet

Assuming no ion loss or recombination in the ionization zone, the current density of the ions flowing away from the cathode can be described as

$$J_{i,p} = -J_i \left(\frac{1-\alpha}{\alpha}\right) = -J_i \tag{27}$$

for $\alpha = 0.5$. The fraction of the ion current to the arc current is therefore

$$\zeta = \left|\frac{J_{i,p}}{J_t}\right| = \left|\frac{I_{i,p}}{I_d}\right| \tag{28}$$

where $I_{i,p}$ is the ion current. Using an empirical formula approximating the gasdynamic accelerating mechanism [31], the mean ion velocity can be estimated with

$$\bar{v}_i \approx 3.5 \left(\frac{5}{3} \frac{\bar{Z} K_b T_{e,p}}{m_i}\right)^{1/2} \tag{29}$$

where $T_{e,p}$ is the electron temperature at which the plasma transitions from LTE to non-LTE conditions as it expands away from the cathode. For simplicity, it is assumed that the electron temperature T_e in the ionization zone (and by inference, also at the sheath edge) is similar in value to $T_{e,p}$, i.e., $T_e \approx T_{e,p}$.

Thruster Performance

The thruster performance parameters that need to be determined by the VAT model are the thrust, thrust-to-power ratio, erosion rate, specific impulse and efficiency. We calculate the thrust (assumed constant during the arc pulse) by using plasma parameters at the plasma jet-ionization zone interface. The following thrust expression is based on that by Polk et al. [4]:

$$F = C_T \left(m_i \frac{\zeta I_d}{e\bar{Z}}\right) \bar{v}_i \tag{30}$$

where C_T is a thrust correction factor to account for plume divergence and thruster geometry and is discussed in more detail here [4]. For a flush electrode configuration and exponential ion distribution, $C_T = 0.64$ [4]. Since ion mass is much larger than electron mass, it is assumed that thrust is mainly due to ion flow.

The cathode erosion rate is estimated by applying a mass flux balance at the cathode surface, where atoms are evaporated and returning ions condense. Assuming all the returning ions condense on the surface, the approximate erosion rate is [20]

$$E_r = \left(\Gamma_{\mathrm{vap}} - \sum_k \frac{J_{i,k}}{Z_k e}\right) \frac{m_n}{J_t} \tag{31}$$

A major limitation of this equation is the exclusion of erosion due to liquid droplet ejection, which may be substantial for certain materials (e.g., lead), high operating arc currents (greater than 500 A) or short pulse lengths (less than 1 μs) [12].

Specific impulse is defined as [4]

$$I_{\mathrm{sp}} = \frac{F}{g E_r I_d} \tag{32}$$

where g is the gravitational acceleration constant. Arc power is defined as

$$P = I_d V_d \tag{33}$$

Thus, the thrust-to-power ratio of the thruster is [4]

$$H = \frac{F}{P} \tag{34}$$

and the thruster efficiency is [4]

$$\eta = \frac{F^2}{2E_r I_d P} \tag{35}$$

It should be noted that specific impulse, thrust-to-power ratio, and efficiency are independent of arc current, which allows the VAT to operate under a wide power range without loss of performance (as long as gross melting of the cathode does not occur from too high an arc current or power duty cycle).

Cathode Surface Energy Flux Balance

The energy flux components that heat and cool the cathode surface, respectively, are grouped as follows

$$q_{\text{heat}} = q_i + q_{\text{er}} + q_J \tag{36}$$

$$q_{\text{cool}} = q_{\text{em}} + q_{\text{vap}} + q_{\text{con}} \tag{37}$$

which are equated to form an energy balance at the cathode surface, i.e., $q_{\text{heat}} = q_{\text{cool}}$. Heat loss due to radiation is small compared to the other energy fluxes and is considered negligible here. The current densities within the sheath region are constant due to the assumption of a collisionless sheath. This allows the energy fluxes at the surface to be determined using the current densities calculated at the sheath edge. The ion bombardment energy flux is described as [11,20,26]

$$q_i = \sum_k \frac{J_{i,k}}{Z_k}\left(W_{i,k} + Z_k V_{\text{cs}} - Z_k \phi_{\text{eff}} + \frac{2K_b T_i}{e} + W_{\text{vap}}\right) \tag{38}$$

where W_{vap} is the material heat of vaporization. Joule heating is approximated as [12,26]

$$q_J \approx \frac{1}{2}\frac{J_t^2 r_s}{\sigma} \tag{39}$$

where the electric conductivity σ of the cathode material is determined by means of the Wiedmann-Franz Law

$$\sigma = \frac{\lambda}{LT_s} \tag{40}$$

where L is the Lorentz number and λ is the thermal conductivity of the cathode material at an approximate molten temperature point. The emitted and returning electron energy flux, respectively, are determined by [12]

$$q_{\text{em}} = J_{\text{em}} \phi_{\text{eff}} \tag{41}$$

$$q_{\text{er}} = J_{\text{er}}\left(\phi_{\text{eff}} + \frac{2K_b T_e}{e}\right) \tag{42}$$

The vaporized atom energy flux is [11,20,23]

$$q_{\text{vap}} = e W_{\text{vap}} \Gamma_{\text{vap}} \tag{43}$$

The heat conduction energy flux is roughly approximated by [12]

$$q_{\text{con}} \approx \frac{\pi}{4}\lambda\left(\frac{T_s - T_m}{r_s}\right) \tag{44}$$

where T_m is the cathode material melting point.

Method of Solution

The following list of nonrefractory materials were studied: aluminum (Al), titanium (Ti), chromium (Cr), iron (Fe), nickel (Ni), copper (Cu), silver (Ag), lead (Pb), and bismuth (Bi). Table 1 lists their material properties and respective experimental values used for model inputs.

An iterative approach is needed to solve the model since the surface temperature is dependent on the (unknown) cathode-spot size, which is governed by the balance of energy flowing in and out of the spot region. To begin, solve for the case of a single cathode spot, i.e., $I_t = I^*$. An assumed spot radius is specified to determine the total current density J_t [Eq. (17)]. A surface temperature T_s is assumed within an appropriate range (e.g., 2500–10,000 K) and used to solve various properties of the arc and plasma jet [Eqs. (1–17)]. An initial plasma density n_p is assumed to find γ [Eqs. (23–26)], which is substituted into Eq. (6). A new plasma density n_p^* is calculated using Eqs. (19–21) and fed back into the sequence of arc and plasma equations [Eqs. (3–17)] for iteration until a convergence criterion is reached, namely

Table 1 Material properties and experimental data of cathode materials under study

Element	Al	Ti	Cr	Fe	Ni	Cu	Ag	Pb	Bi
Atomic no.	13	22	24	26	28	29	47	82	83
Mass, g/mol [32]	26.981	47.9	52	55.845	58.71	63.55	107.87	207.2	208.98
$W_{i,1}$, eV [19]	5.99	6.83	6.77	7.9	7.64	7.73	7.58	7.42	7.29
$W_{i,2}$, eV [19]	18.83	13.76	16.49	16.19	18.17	20.29	21.49	15.03	16.69
$W_{i,3}$, eV [19]	28.45	27.49	30.96	30.65	35.19	36.84	34.83	——	——
$W_{i,4}$, eV [19]	——	——	49.16	——	——	57.38	60.52	——	——
λ, W/mK [33]	125.6 [34]	24.5	49.4	32.1	58.2 [34]	339	361	29.8 [34]	7.04
W_{vap}, eV [32]	3.04	4.40	3.51	3.60	3.92	3.11	2.64	1.84	1.66
W_{CE}, eV/atom [35]	3.39	4.85	4.1	4.28	4.44	3.49	2.95	2.03	2.18
ϕ, eV [36]	4.06	4.33	4.5	4.67	5	4.53	4.52	4.25	4.34
K_1 [22]	11.79	12.5	12.94	12.44	12.75	11.96	11.85	10.77	11.18
K_2 [22]	15,940	23,200	20,000	19,970	20,960	16,980	14,270	9710	9530
B_0 [37]	0.5	2	3	4	4	0.5	0.5	0	1.5
B_1 [37]	0	1.5	2.5	4.5	2.5	0	0	0.5	0
T_b, K [32]	2792	3560	2944	3134	3186	2835	2435	2022	1837
T_m, K [32]	933.4	1933	2130	1808	1726	1357.8	1234	600.8	544.7
f_1, % [18]	38	11	10	25	30	16	13	36	83
f_2, % [18]	51	75	68	68	64	63	61	64	17
f_3, % [18]	11	14	21	7	6	20	25	0	0
f_4, % [18]	0	0	1	0	0	1	1	0	0
$\bar{Z}$	1.73	2.03	2.13	1.82	1.76	2.06	2.14	1.64	1.17
T_e, eV [19]	3.1	3.2	3.4	3.4	3	3.5	4	2	1.8
I^*, A [3]	30–50	70	30–50	60–100	——	75–100	60–100	5–9	3–5

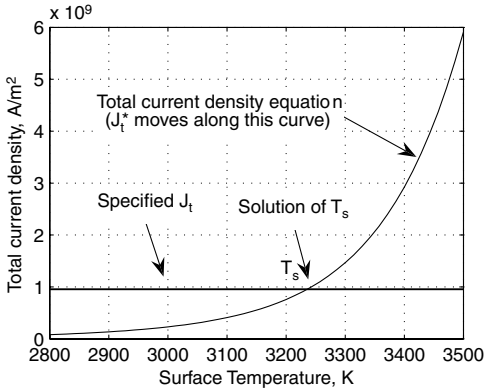

Fig. 2 Example of the intersection of calculated and specified total current densities to solve for the surface temperature.

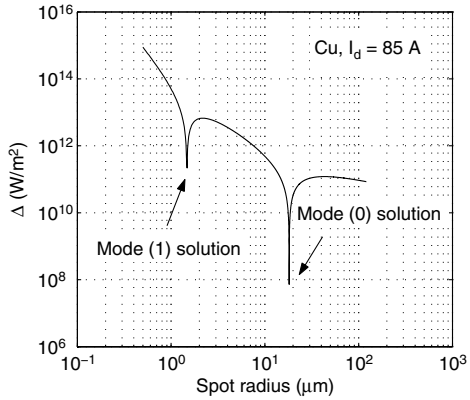

Fig. 3 Convergence of energy flux balance showing possible mode 0 and 1 solutions.

$$\left|\frac{n_p^* - n_p}{n_p}\right| \leq 10^{-6} \tag{45}$$

Once the plasma density is found, the total current density J_t^* can be found with Eq. (16) and compared to the specified J_t (Fig. 2). Using a modified *bisection method*, T_s is varied until the specified and calculated total current densities are suitably close in value (change in $T_s < 0.1$ K), resulting in the convergence criterion:

$$\left|\frac{J_t^* - J_t}{J_t}\right| \leq 10^{-3} \tag{46}$$

At this point, there is a unique set of arc and plasma properties for the assumed spot radius. To complete the solution, an energy flux balance at the cathode-spot surface [Eqs. (36) and (37)] is used to find the correct spot radius (r_s plays a direct role in Joule heating and heat conduction). Calculation of the energy flux terms [Eqs. (38–44)] results in a comparison of the conduction energy flux terms obtained from Eq. (44) and rearrangement of the energy flux balance, i.e., $\Delta = |q_{\text{con}}^* - q_{\text{con}}|$. The entire solution process was repeated for a range of radii, starting at 0.2 μm and increasing in 0.02 μm increments until the smallest difference between the conduction

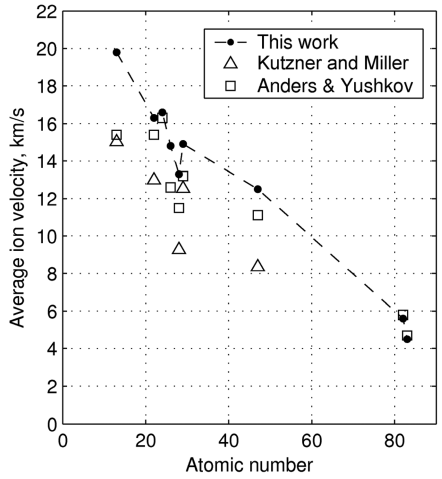

Fig. 4 Comparison of ion velocities for this work, experimental results by Kutzner and Miller [44] (as cited by Boxman et al. [12]), and Anders and Yushkov [35] (dashed line is only a visual aid).

Table 2 Comparison of predicted and published values of maximum arc spot current (I^*, A) for Ti, Cr, Fe, Ni, and Bi

Element	This work	Harris, as cited by Lafferty [3]
Ti	60	70
Cr	36	30–50
Fe	20	60–100
Ni	57	——
Bi	2	3–5

Table 4 Comparison of ion-to-arc current ratio (ζ, %) with published data

Element	This work	Anders et al. [39]	Kimblin [40]
Al	11.8	11.2	
Ti	8.8	9.7	8.0
Cr	5.8	——	7.5
Fe	7.8	——	8.0
Ni	7.8	——	——
Cu	11.2	11.4	——
Ag	5.9	——	8.0
Pb	13.6	14.3	——
Bi	6.8	10.2	——

Table 3 Model results for a single cathode spot

Element	Al	Ti	Cr	Fe	Ni	Cu	Ag	Pb	Bi
I_t ($\leq I^*$), A	40	60	36	20	57	85	80	7	2
V_d, V	20	22.5	21.2	21.5	21.8	20.2	19.3	17.7	18.0
r_s, μm	13.5	27.4	6.6	6.5	8.5	18.2	11.0	8.3	2.2
T_s, K	3906	4393	4088	4530	4712	4164	3801	3411	3504
E, 10^9 V/m	2.83	1.82[a]	4.88	4.17	5.43	3.87	5.15	3.30	4.34
γ	0.99	1.00	0.98	0.98	0.96	0.99	0.99	0.89	0.75
n_p, 10^{26} m^{-3}	0.66	0.26	1.89	1.33	2.35	1.20	2.06	1.17	2.04
J_{em}, 10^{10} A/m^2	6.42	2.38	26.17	14.47	23.51	8.29	24.62	2.86	12.39
q_i, 10^{11} W/m^2	2.19	0.61	4.24	3.19	5.55	2.56	3.42	0.99	2.09
v_i, km/s	19.8	16.3	16.6	14.8	13.3	14.9	12.5	5.6	4.5

[a]Although the value of E is slightly below the limits of validity for the approximation equation for J_{em}, the resulting current density is still roughly similar in value to that obtained by Murphy and Good's [28] equation (see Fig. 48 and Table 12 in Chapter 3 of Boxman et al. [12]).

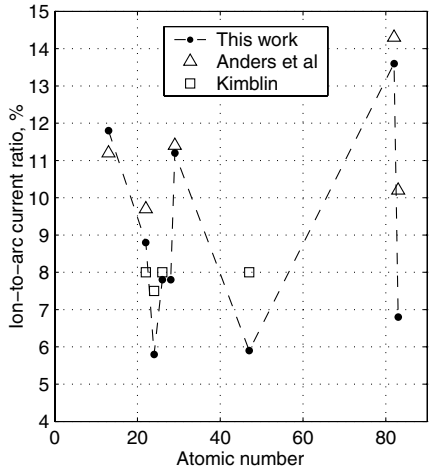

Fig. 5 Ion-to-arc current ratios for this work, experiments by Anders et al. [39] and Kimblin [40].

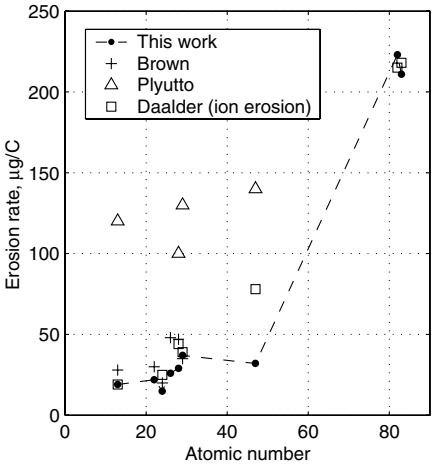

Fig. 6 Erosion rate for this work, experiments by Brown and Shiraishi [41], Plyutto and Daalder (as cited by Boxman et al. [12]), and Daalder [42,43] (ion erosion only).

terms was found (typically 6–8 orders of magnitude smaller than the peak difference).

Interestingly, there are actually *two* solutions that emerge from the energy flux balance (Fig. 3). This result reflects the two conditions that a vacuum arc can exist at, namely mode 0 and mode 1 [3]. Mode 1 is characterized by more intense conditions: that is, larger values of T_s, E, J_t, etc., compared to mode 0, suggesting that mode 1 should have a smaller spot radius than mode 0 to account for the larger current density and other arc properties. For example, in the convergence graph in Fig. 3, the first convergence point occurs around $r_s = 1$–2 μm and the second at around $r_s = 10$ μm, which produces the expected order of magnitude difference in arc properties. Nonrefractory metals usually prefer operating at mode 0 due to the lower arc voltage requirement and greater arc stability than mode 1 [3]. Hence, the larger spot radius solution is chosen. Thruster performance is found from solving Eqs. (30–35).

Results and Discussion

It was found for some materials (e.g., Ti, Cr) that possible model solutions only existed for arc spot currents close to the published values of I^* [3]. As I_t approaches I^*, the mode 0 and mode 1 cathode-spot radius solutions of these materials converge to a single intermediate solution at a specific arc spot current value. Beyond this arc spot current value, however, no solution is attained. It is interesting to note that these materials have relatively moderate thermal conductivities (7–60 W/mK). Therefore, one possible interpretation is that beyond this maximum arc spot current, conditions within the arc become unsuitable for a stable arc to be maintained because heat at the cathode surface cannot dissipate fast enough. The vacuum arc resolves this by forming proportionately more spots to carry the additional arc current that the single spot cannot carry on its own. Thus, the model was able to predict values of I^* that were in good agreement with published data [with the exception of Fe (see Table 2)]. However, predicted values of I^* can vary significantly due to its strong dependence on the values of thermal conductivity, which carries a high degree of variation between grades of the same material and over the molten temperature range.

On the other hand, materials such as Al, Cu, Ag, and Pb have possible model solutions for arc spot currents much greater than their respective I^* values by factors of about 8–20 depending on the material. All these materials (with the exception of Pb) have relatively high thermal conductivities (120–360 W/mK), which suggests that they are capable of dissipating the heat generated from such high arc currents and that I^* is governed by another process.

Table 3 is a summary of model results obtained for a single cathode spot. Published and predicted values of I^* have been used when relevant. Results are generally in good agreement with literature, e.g., for copper [4,11,26,38], $V_d = 15$–20 V, $r_s \sim 25$ μm, $T_s \approx 4000$ K, $E \sim 2 \times 10^9$ V/m, $\gamma \approx 1$, $n_p \approx 10^{26}$ m^{-3}, $J_t \sim 10^{10}$ A/m^2, $q_i \sim 10^{12}$ W/m^2, and $v_i \approx 13$ km/s.

Figure 4 compares predicted average ion velocities with published experimental data [12,35]. General trends are in agreement, with velocity values for the lighter elements being overpredicted by up to roughly 30% (Al). However, some discrepancies also exist in experimental values by up to roughly 35% (Ag).

Table 4 and Fig. 5 compares ion-to-arc current ratios of this work to those obtained by experiment [39,40]. Predicted values of ζ show surprisingly good agreement with measured values to within 10% difference for most materials with the exception of Cr (29%), Ag (36%), and Bi (50%).

Figure 6 compares predicted values of erosion rate with experimental values. Results are in good agreement for most materials when compared to values by Brown and Shiraishi's [41] (except for Pb) and Daalder's [42,43] results and described in [12]. A

Table 5 Thruster performance compared with published data

	This work				Polk et al. [4]			
Element	H, μN/W	I_{sp}, s	E_r, μg/C	η, %	H, μN/W	I_{sp}, s	E_r, μg/C	η, %
Al	12.11	1274	19	7.6	7.03	604	28	2.1
Ti	9.99	1060	22	5.2	12.77	924	30	5.8
Cr	7.32	1046	15	3.8	14.28	1666	20	11.7
Fe	10.88	934	26	5.0	11.01	531	48	2.9
Ni	10.56	797	29	4.1	12.24	544	47	3.3
Cu	17.03	950	37	7.9	11.65	794	35	4.5
Ag	12.87	795	32	5.0	18.43	317	140	2.9
Pb	35.91	291	223	5.1	30.39	94	510	1.4
Bi	19.87	173	211	1.7	33.20			

comparison with Plyutto's results, as described in [12], however, shows an underpredicted E_r by a factor of at about 2–4. This may be due to macroparticle ejection that contributes significantly toward erosion during high arc currents and high overall cathode temperatures. The model's results agree well with Daadler's [42,43] ion erosion rate only because we have not considered such macroparticle ejection. Therefore, predicted E_r values are most accurate for materials that exhibit low macroparticle ejection.

Table 5 and Figs. 7–10 compare thruster performance results with that obtained by Polk et al.'s [4] semi-empirical model. It was found that materials with a good thrust-to-power ratio do not necessarily have good efficiency due to a large erosion rate. Interestingly, Cu has the best all-round performance with a thrust-to-power ratio of 17.03 μN/W, specific impulse of 950 s, and the highest efficiency of 7.9%. Other materials that deliver good performance are Al, Ti, Fe, Ni, and Ag. Thrust results in Figs. 7 and 8 are in general agreement with literature, with discrepancies being mainly credited to Polk et al.'s [4] assumption of $\zeta = 0.1$ for all materials and our overestimated average ion velocities. Differences in specific impulses and efficiencies are compounded by differences occurring in ζ, v_i and E_r. The similarity between data trend lines in Figs. 5, 7, 8, and 10 shows that ζ has a significant effect on thrust ($F \propto \zeta$) and efficiency ($\eta \propto \zeta^2$), especially at higher arc currents. However, erosion rates are less influenced by values of ζ. Model results also appear to show that lighter elements have higher ion velocities, lower erosion rates, and higher I_{sp} than the heavy elements. Element mass only gives heavier elements an advantage in terms of thrust. Thus, we find that the choice of a suitable cathode for a VAT is not so simple and depends heavily on the propulsion application as well as thrust, power, mass, and contamination constraints and mission objectives.

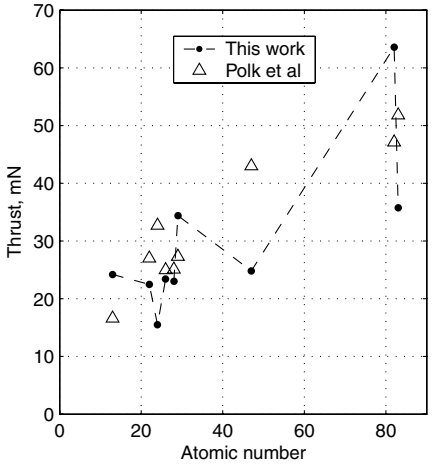

Fig. 7 Thrust results for this work and semi-empirical model by Polk et al. [4] ($I_d = 100$ A).

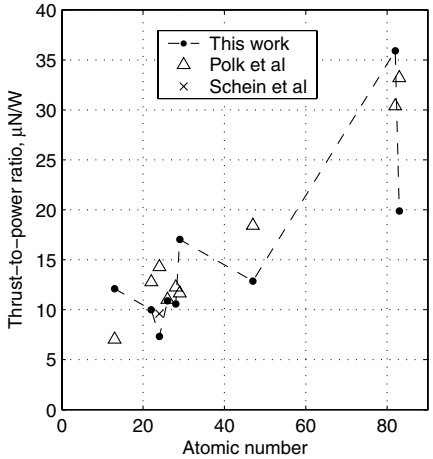

Fig. 8 Thrust-to-power ratios for this work, semi-empirical model by Polk et al. [4] and experimental result by Schein et al. [45] (Cr cathode).

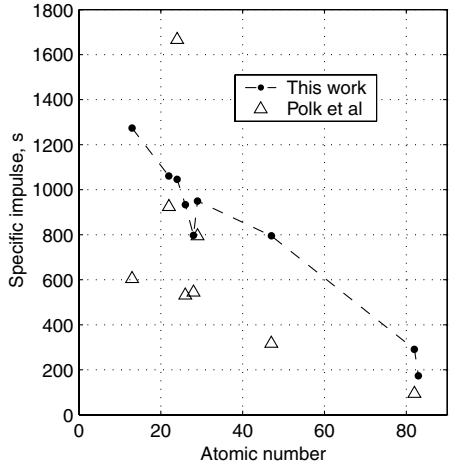

Fig. 9 Specific impulse for this work and semi-empirical model by Polk et al. [4].

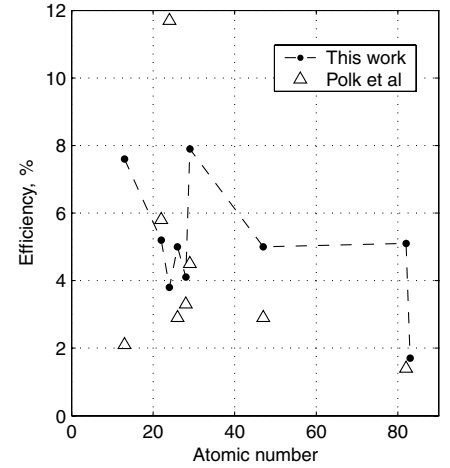

Fig. 10 Thruster efficiency for this work and semi-empirical model by Polk et al. [4].

Conclusions

Despite the use of a conventional-based cathode-spot model with many simplifying assumptions, values for spot radius, surface temperature, electric field, current densities, plasma densities, and energy fluxes are in good agreement with other models and experiments. Predictions of maximum arc spot current for Ti, Cr, and Bi were also in excellent agreement with literature. The model reflects the material dependency of ζ contained in published experimental results with most predictions to within 10%. It is emphasized that the ion-to-arc current ratio should be determined as accurately as possible due to its significant effect on thruster performance. In conclusion, the simplified VAT model has successfully predicted thruster performance comparable to that of semi-empirical modelling and presented a wide range of possible cathode performance.

However, a drawback of the model is the exclusion of macroparticle ejection and the inability to obtain a solution for refractory metals (e.g., tungsten) even though vacuum arcs on such materials are possible in practice. Modifications to the cathode-spot model as described by Lafferty [3], Beilis [8], and Boxman et al. [12] may be implemented to address this issue. Future improvements to the model include the effect of macroparticle ejection on the erosion rate and plasma jet and a better estimate of the average ion velocity. It is also

recommended that predictions and measurements of ζ be extended to additional cathode materials to further validate the model.

Acknowledgment

Funding for this work was provided by the University of Stellenbosch.

References

[1] Schein, J., Qi, N., Binder, R., Krishnan, M., Ziemer, J. K., Polk, J. E., and Anders, A., "Inductive Energy Storage Driven Vacuum Arc Thruster," *Review of Scientific Instruments*, Vol. 73, No. 2, 2002, pp. 925–927. doi:10.1063/1.1428784

[2] Schein, J., Gerhan, A. N., Woo, R. L., Au, M. Y., and Krishnan, M., "Vacuum Arc Plasma Thrusters with Inductive Energy Storage Driver," U.S. Patent Publication No. 2007/0045248 A1, March 2007.

[3] Lafferty, J. M. (ed.), *Vacuum Arcs–Theory and Application*, Wiley, New York, 1980, Chaps. 4, 7.

[4] Polk, J. E., Sekerak, M., Ziemer, J. K., Schein, J., Qi, N., and Anders, A., "A Theoretical Analysis of Vacuum Arc Thruster and Vacuum Arc Ion Thruster Performance," *IEEE Transactions on Plasma Science*, Vol. 36, No. 5, 2008, pp. 2167–2179. doi:10.1109/TPS.2008.2004374

[5] Statom, T. K., "Vacuum Arc Nano-Thruster Cathode Performance for Nano-Satellites," 34th AIAA Plasmadynamics and Lasers Conference, AIAA Paper 2003-4291, Orlando, FL, 23–26 June 2003.

[6] Keidar, M., Schein, J., Wilson, K., Gerhan, A., Au, M., Tang, B., et al., "Magnetically Enhanced Vacuum Arc Thruster," *Plasma Sources Science and Technology* , Vol. 14, No. 4, 2005, pp. 661–669. doi:10.1088/0963-0252/14/4/004

[7] Rysanek, F., and Burton, R. L., "Charging of Macroparticles in a Pulsed Vacuum Arc Discharge," *IEEE Transactions on Plasma Science*, Vol. 36, No. 5, 2008, pp. 2147–2162. doi:10.1109/TPS.2008.2000880

[8] Beilis, I. I., "Modeling of a Microscale Short Vacuum Arc for a Space Propulsion Thruster," *IEEE Transactions on Plasma Science*, Vol. 36, No. 5, 2008, pp. 2163–2166. doi:10.1109/TPS.2008.2004217

[9] Anders, A., *Cathodic Arcs: From Fractal Spots to Energetic Condensation*, Springer, New York, 2008, Chap. 3.

[10] Hantzsche, E., "Mysteries of the Arc Cathode Spot: A Retrospective Glance," *IEEE Transactions on Plasma Science*, Vol. 31, No. 5, 2003, pp. 799–808. doi:10.1109/TPS.2003.818412

[11] Hantzsche, E., "The State of the Theory of Vacuum Arc Cathodes," *Contributions to Plasma Physics*, Vol. 23, No. 1, 1983, pp. 77–94. doi:10.1002/ctpp.19830230108

[12] Boxman, R. L., Martin, P. J., Sanders, D. M., (eds.), *Handbook of Vacuum Arc Science and Technology–Fundamentals and Applications*, Noyes, New York, 1995, Chaps. 3–4.

[13] Rysanek, F., and Burton, R., "Acceleration Mechanisms in a Vacuum Arc Thruster," 39th AIAA/ASME/SAE/ASEE Joint Propulsion Conference and Exhibit, AIAA Paper 2003-4565, Huntsville, AL, 20–23 July 2003.

[14] Hantzsche, E., "Theory of the Expanding Plasma of Vacuum Arcs," *Journal of Physics D: Applied Physics*, Vol. 24, No. 8, 1991, pp. 1339–1353. doi:10.1088/0022-3727/24/8/017

[15] Anders, S., Anders, A., Yu, K. M., Yao, X. Y., and Brown, I. G., "On the Macroparticle Flux from Vacuum Arc Cathode Spots," *IEEE Transactions on Plasma Science*, Vol. 21, No. 5, 1993, pp. 440–446. doi:10.1109/27.249623

[16] Messaad, M., Belarbi, A. W., Lefort, A., and Abbaoui, M., "Model for a Low Current Vacuum Arc Cathode Region–Effect of the Electronic Temperature," *Acta Electrotechnica et Informatica*, Vol. 6, No. 3, 2006, pp. 1–8.

[17] Benilov, M. S., "A Self-Consistent Analytical Model of Arc Spots on Electrodes," *IEEE Transactions on Plasma Science*, Vol. 22, No. 1, 1994, pp. 73–77. doi:10.1109/27.281554

[18] Brown, I. G., "Vacuum Arc Ion Sources," *Review of Scientific Instruments*, Vol. 65, No. 10, 1994, pp. 3061–3081. doi:10.1063/1.1144756

[19] Anders, A., "Ion Charge State Distributions of Vacuum Arc Plasmas: The Origin of Species," *Physical Review E (Statistical Physics, Plasmas, Fluids, and Related Interdisciplinary Topics)*, Vol. 55, No. 1, 1997, pp. 969–981. doi:10.1103/PhysRevE.55.969

[20] Coulombe, S., "A Model of the Electric Arc Attachment on Non-Refractory (Cold) Cathodes," Ph.D. Dissertation, Department of Chemical Engineering, McGill Univ., Montrèal, 1997.

[21] Anders, A., Yotsombat, B., and Binder, R., "Correlation Between Cathode Properties, Burning Voltage, and Plasma Parameters of Vacuum Arcs," *Journal of Applied Physics*, Vol. 89, No. 12, 2001, pp. 7764–7771. doi:10.1063/1.1371276

[22] Roth, A., "Physico-Chemical Phenomena in Vacuum Techniques," *Vacuum Technology*, North-Holland, Amsterdam, 1976, pp. 149–150.

[23] Mitterauer, J., and Till, P., "Computer Simulation of the Dynamics of Plasma-Surface Interactions in Vacuum Arc Cathode Spots," *IEEE Transactions on Plasma Science*, Vol. 15, No. 5, 1987, pp. 488–501. doi:10.1109/TPS.1987.4316742

[24] Rethfeld, B., Wendelstorf, J., Klein, T., and Simon, G., "A Self-Consistent Model for the Cathode Fall Region of an Electric Arc," *Journal of Physics D: Applied Physics*, Vol. 29, No. 1, 1996, pp. 121–128. doi:10.1088/0022-3727/29/1/021

[25] Riemann, K.-U., "Theory of the Cathode Sheath in a Vacuum Arc," *IEEE Transactions on Plasma Science*, Vol. 17, No. 5, 1989, pp. 641–643. doi:10.1109/27.41172

[26] Rossignol, J., Clain, S., and Abbaoui, M., "The Modelling of the Cathode Sheath of an Electrical Arc in Vacuum," *Journal of Physics D: Applied Physics*, Vol. 36, No. 13, 2003, pp. 1495–1503. doi:10.1088/0022-3727/36/13/311

[27] Bolotov, A., Kozyrev, A., and Korolev, Y., "A Physical Model of the Low-Current-Density Vacuum Arc," *IEEE Transactions on Plasma Science*, Vol. 23, No. 6, 1995, pp. 884–891. doi:10.1109/27.476470

[28] Murphy, E. L., and Good, R. H., "Thermionic Emission, Field Emission, and the Transition Region," *Physical Review*, Vol. 102, No. 6, 1956, pp. 1464–1473. doi:10.1103/PhysRev.102.1464

[29] Pfender, E., "Electric Arcs and Arc Gas Heaters," *Gaseous Electronics: Vol. 1–Electrical Discharges*, edited by M. N. Hirsh, and H. J. Oskam, Academic Press, London, 1978, pp. 301–304.

[30] Cambel, A. B., "Thermodynamics of Real Gases," *Plasma Physics and Magnetofluidmechanics*, McGraw–Hill Series in Missile and Space Technology, McGraw–Hill, New York, 1963, pp. 109, 113–119, 124, 143–145.

[31] Yushkov, G. Y., Bugaev, A. S., Krinberg, I. A., and Oks, E. M., "On a Mechanism of Ion Acceleration in Vacuum Arc-Discharge Plasma," *Doklady Physics*, Vol. 46, No. 5, 2001, pp. 307–309. doi:10.1134/1.1378090

[32] *WebElements* [online], www.webelements.com [retrieved 25 July 2009].

[33] Incropera, F. P., and Dewitt, D. P., "Thermophysical Properties of Matter," *Fundamentals of Heat and Mass Transfer*, 4th ed., Wiley, New York, App. A.

[34] Rohsenow, W. M. Hartnett, J. P., Cho, Y. I., "Thermophysical Properties," *Handbook of Heat Transfer*, 3rd ed., McGraw–Hill Professional, New York, 1998, Chap. 2, pp. 251–255.

[35] Anders, A., and Yushkov, G. Y., "Ion Flux from Vacuum Arc Cathode Spots in the Absence and Presence of a Magnetic Field," *Journal of Applied Physics*, Vol. 91, No. 8, 2002, pp. 4824–4832. doi:10.1063/1.1459619

[36] Lide, D. R., *CRC Handbook of Chemistry and Physics 2008–2009*, 89th ed., CRC Press, Boca Raton, FL, 2008, pp. 12–114.

[37] Sansonetti, J. E., Martin, W. C., and Young, S. L., *Handbook of Basic Atomic Spectroscopic Data (Version 1.1.2)*, National Inst. of Standards and Technology, http://physics.nist.gov/Handbook [retrieved 25 July 2009].

[38] Jüttner, B., "Cathode Spots of Electric Arcs," *Journal of Physics D: Applied Physics*, Vol. 34, No. 17, 2001, pp. 103–123. doi:10.1088/0022-3727/34/17/202

[39] Anders, A., Oks, E. M., Yushkov, G. Y., Savkin, K. P., Brown, I. G., and Nikolaev, A. G., "Measurements of the Total Ion Flux from Vacuum Arc Cathode Spots," *IEEE Transactions on Plasma Science*, Vol. 33, No. 5, 2005, pp. 1532–1536. doi:10.1109/TPS.2005.856502

[40] Kimblin, C. W., "Erosion and Ionization in the Cathode Spot Region of a Vacuum Arc," *Journal of Applied Physics*, Vol. 44, No. 7, 1973, pp. 3074–3081. doi:10.1063/1.1662710

[41] Brown, I. G., and Shiraishi, H., "Cathode Erosion Rates in Vacuum-Arc Discharges," *IEEE Transactions on Plasma Science*, Vol. 18, No. 1,

1990, pp. 170–171.
doi:10.1109/27.45521

[42] Daalder, J. E., "Erosion and the Origin of Charged and Neutral Species in Vacuum Arcs," *Journal of Physics D: Applied Physics*, Vol. 8, No. 14, 1975, pp. 1647–1659.
doi:10.1088/0022-3727/8/14/009

[43] Daalder, J. E., "Components of Cathode Erosion in Vacuum Arcs," *Journal of Physics D: Applied Physics*, Vol. 9, No. 16, 1976, pp. 2379–2395.
doi:10.1088/0022-3727/9/16/009

[44] Kutzner, J., and Miller, H. C., "Integrated Ion Flux Emitted from the Cathode Spot Region of a Diffuse Vacuum Arc," *Journal of Physics D: Applied Physics*, Vol. 25, No. 4, 1992, pp. 686–693.
doi:10.1088/0022-3727/25/4/015

[45] Schein, J., Krishnan, M., Polk, J., and Ziemer, J., "Adding a 'Throttle' to a Clustered Vacuum Arc Thruster," *Nanotech Conference*, AIAA Paper 2002-5716, Houston, TX, 2002.

A. Gallimore
Associate Editor